Acute exposure of minimally ox-LDL elicits survival responses by downregulating the mediators of NLRP3 inflammasome in cultured RAW 264.7 macrophages

Finosh Thankam (fthankam@westernu.edu)
Western University of Health Sciences https://orcid.org/0000-0001-7285-9808
Bisma Khwaja
Western University of Health Sciences
Megan Nguyen
Western University of Health Sciences
Osama Ahsan
Western University of Health Sciences
Devendra Agrawal
Western University of Health Sciences

Research Article

Keywords: Atherosclerosis, Oxidized-LDL, Lipid-burden, Macrophages, Sterile inflammation

Posted Date: March 21st, 2022

DOI: https://doi.org/10.21203/rs.3.rs-1460377/v1

Abstract

Lipid burden in macrophages driven by oxidized LDL (oxLDL) accelerates the foam cell formation and the activation of sterile inflammatory responses aggravating the atherosclerosis. However, there is limited information on the mediators and the pathways involved in the possible survival responses, especially at the initial phase, by lipid-burden in macrophage cells on encountering oxLDL. Hence, the present study was designed to assess the expression status of major mediators involved in the NLRP3 inflammasome pathway of sterile inflammation and the cellular responses in oxLDL-challenged cultured RAW 264.7 macrophage cells. The ox-LDL-treated RAW 264.7 macrophage cells displayed a decreased expression of the key sterile inflammatory mediators, TLR4, TLR2, ASC, NLRP3 and IL-18 at the protein and transcript level; however, displayed increased level of IL-1β, RAGE and TREM1 at the protein level. The biological responses including lipid uptake, lipid peroxidation, superoxide production and mitochondrial membrane potential were significantly decreased in oxLDL-treated macrophages. Moreover, cellular hypertrophy and mitochondrial density were significantly decreased in the oxLDL-treated macrophages compared to the control. Overall, the findings revealed that the expression status of key sterile mediators and the macrophage response during the initial phase of oxLDL exposure tend toward the prevention of inflammation. Further understanding would open novel translational opportunities in the management of atherosclerosis.

Introduction

Lipid burden in macrophages driven by low-density lipoprotein (LDL) and oxidized LDL (oxLDL) accelerate the foam cell formation in aggravated atherosclerosis. The oxLDL act as potential damage-associated molecular patterns (DAMP) triggering the sterile inflammatory responses leading to the release and activation of the pro-inflammatory cytokines IL-1β and IL-18 via nucleotide–binding domain and leucine-rich repeat (NLR)–containing family and pyrin domain (PYD)–containing 3 (NLRP3) inflammasome activation [1] [2]. Despite the anti-inflammatory phenotypes, the macrophages are usually polarized towards inflammatory phenotypes in the pro-atheromatous milieu created by oxLDL contributing substantially to vascular inflammation and atherosclerosis pathology [3]. Importantly, unresolving inflammation persists in atherosclerosis resulting in defective efferocytosis promoting the formation of the necrotic core; however, the underlying molecular mechanisms are currently unknown [1]. Moreover, the sterile inflammatory cytokines, IL-1β and IL-18, are proteolytically activated by NLRP3 inflammasome which is composed of the adaptor protein apoptosis-associated speck-like protein containing a CARD (ASC) and the downstream effector caspase-1 [4].

The sterile inflammatory episodes triggered by oxLDL activate the downstream inflammatory signaling predominantly through the activation of the cell surface receptors TLR4 and TLR2 [5]; however, signaling via triggering receptors expressed on myeloid cells (TREM1) and receptors for advanced glycation end products (RAGE) have been involved in the activation of inflammasome in multiple cell types [5] [6]. Research on atherosclerosis, a chronic inflammatory disease, has been focused on the long-term impact of LDL and oxLDL in the progression of pathology using translationally-relevant experimental models.

However, the literature regarding the possible survival responses, especially at the initial phase, by the lipid-burdened macrophage cells on encountering LDL/oxLDL is currently unavailable. Interestingly, a recent seminal study reported that LDL strongly reduced the proinflammatory responses by inhibiting the NLRP3 inflammasome in human macrophages whereas oxLDL displayed superior anti-inflammatory effects suggesting the possible alternative mechanisms [2]. Hence, it is reasonable that the macrophages elicit multiple survival responses during the acute phase of LDL/oxLDL burden. On this background, the present study was designed to assess the expression status of major mediators involved in the NLRP3 inflammasome pathway of sterile inflammation and the cellular responses in LDL/oxLDL-challenged cultured RAW 264.7 macrophage cells.

Methodology

Culture, maintenance, and treatment of RAW 264.7 cells

Mouse macrophage cell line RAW 264.7 was procured from American Type Cell Culture (ATCC-TIB-71) and maintained in high glucose DMEM with 10% fetal bovine serum (FBS) (Cat# 30-2020, ATCC), standard culture conditions (5% CO_2, 37^oC, and antibiotics). Upon 70-80% confluency the cells were split using cell scraper by retaining one-third culture media and replenishing two-third fresh media. LDL was isolated from hyperlipidemic swine plasma and minimally ox-LDL was prepared by controlled oxidation using 5μM $CuSO_4$ following the previously reported protocol [7] [8]. The level of oxidation was confirmed by the level of TBARS as determined by ELISA kit (CAYMAN CHEMICAL, Cat#: 10009055). The cells were treated with 200 μg/ml oxLDL and 400 μg/ml LDL in serum-free media for the investigation, and the cells treated with 100 μg/ml lipopolyscaccharide (LPS from E. coli (L3024, Sigma) and the untreated cells were used as treatment and comparison controls, respectively.

Immunofluorescence

The cells were cultured in 8-well chamber slides and the expression of protein biomarkers was determined using immunostaining following our previous protocols [9]. Primary antibodies (1:400 dilution) against TLR2 (ab213676), TLR4 (ab13556), HMGB1 (ab11354), RAGE (ab37647), ASC (ab175449), NLRP3 (ab214185), Caspase-1 (ab74279), IL-1β (ab156791), TREM1 (ab200729), NF-κB (ab86299) and IL-18 (ab106939) were used for staining and respective fluorochrome conjugated secondary antibodies (1:400) were used for detection. Nuclei were counterstained with 4',6-diamidino-2-phenylindole (DAPI) and imaged using a fluorescent slide scanner microscope (Leica Thunder, Germany). The experiments were performed with a negative control for fixing the exposure time and to minimize the background. The mean fluorescence intensity (MFI) normalized with the number of nuclei was used to calculate the $\log_2$ fold-change (FC) following our previously reported protocol [10].

Lipid droplets staining

Intracellular lipid droplets were stained using LipidSpot™ 488 dye (Cat# 70065, Biotium) in the RAW 264.7 cells cultured in 8-well chamber slides following the manufacturer's instructions. Post-treatment cells were incubated with the dye for 30 min at 37^0C and the live cell imaging was performed using a fluorescent microscope (Leica Thunder) under blue filter. The MFI was quantified, and the results were represented as $\log_2$ FC as mentioned above.

Lipid Peroxidation Assay

Lipid peroxidation following the treatment with LDL and oxLDL on RAW 264.7 macrophages grown in chamber slides was assessed using Image-iT Lipid Peroxidation kit (C10445, Life technologies) according to the manufacturer's instructions. Following the treatment, the cells were washed with serum-free DMEM and incubated with 200µl of Image-iT® Lipid Peroxidation Sensor (10mM in DMSO) for 30 minutes at 37^oC, washed with serum-free DMEM, and imaged under fluorescence slide scanner (Leica Thunder) at 590 nm and 510 nm. The cells treated with LPS (100µM) were used as treatment control and the untreated cells were used as controls. The ratio of the emission fluorescence intensities at 590nm to 510nm reflects the extent of lipid peroxidation. RAW 264.7 cells treated with cumene hydroperoxide (CuP) at a final concentration of 100µM for 2 hours at 37°C in each group served as the positive control.

Mitochondrial density

The mitochondrial density in the post-treatment RAW 264.7 cells cultured in 8-well chamber slides were determined using MitoView™ Green (Cat# 70054, Biotium) following the manufacturer's instructions. The cells were incubated with the 100 nM dye for 15 min at 37^0C and the live cell imaging was performed using a fluorescent microscope (Leica Thunder) under blue filter. The MFI proportionate with the mitochondrial content and the results were represented as $\log_2$ FC.

Mitochondrial superoxide

The status of ROS in the RAW 264.7 cells was examined by determining mitochondrial superoxide using MitoSOX Red (M36008, Invitrogen) following our published protocol [11]. The RAW 264.7 cells under treatment were cultured in 8-well chamber slides and were treated with 5µM MitoSOX Red reagent for 10 min and the live cell imaging was performed using a fluorescent microscope (Leica Thunder) mounting in DMEM (serum free). The untreated cells served as the control. MFI values were quantified, and the results were represented as Log_2 FC.

Mitochondrial pore transition

The mitochondrial pore integrity was assessed in the RAW 264.7 cells in various treatment groups using Image-iT LIVE mitochondrial transition pore assay kit (I35103, Invitrogen) following our previously reported protocol [11]. The cells were incubated in 200µl labeling solution containing 1µl each of 1mM calcein AM, 200µM MitoTracker Red, 1mM Hoechst 33342, and 1mM $CoCl_2$ in serum free DMEM at 37^oC for 15 min, washed with serum-free DMEM and immediately imaged under fluorescence slide scanner (Leica Thunder). The untreated cells were used as control and the results are presented as Log_2 FC with respect to the control.

Microtubule staining and cell spreading

The microtubule integrity was assessed in the RAW 264.7 cells using ViaFluor 488 Live Cell Microtubule Stain kit (70062-T, bioitum) following the manufacturer's instructions. Following the treatment, the cells were washed with serum-free DMEM, incubated in 200µl probe-containing medium (1µl/ml) at 37^oC for 30 min, washed with serum-free DMEM and immediately imaged under fluorescence slide scanner (Leica Thunder). The untreated cells were used as control and the experiments were run in triplicate. Individual cells from the images were randomly assessed for the area (n=30) and perimeter (n=30) to examine the cell spreading using ImageJ software. The results are expressed as Log_2 FC with respect to control.

Gene expression

The RAW 264.7 cells were treated as mentioned above, total cellular RNA was isolated using the trizol method, and cDNA was synthesized using 1µg RNA from each group using cDNA synthesis kit (Promega) following the manufacturer's protocol. The mRNA transcripts for the genes TLR2, TLR4, IL-18, IL-1β, ASC, and NLRP3 were amplified by real-time PCR (Applied Biosystems, CA, U.S.A.) using SYBR Green chemistry employing appropriate forward and reverse primers (**Table 1)** following the program detailed in our previous protocol [12]. The GAPDH was used as a housekeeping reference gene. The mRNA expression was quantified by $2^{\wedge-\Delta\Delta CT}$ method with respect to GAPDH and the results are presented as Log_2 FC with respect to normal control.

Table 1

List of primers used in qRT-PCR

Primers	Sequence (3’-5’)
ASC (F)	TGCCAGGGTCACAGAAGTGG
ASC (R)	CTTCAAGGCCTGGAGGAGGG
IL-1B (F)	GCCACCTTTTGACAGTGATGAGA
IL-1B (R)	TGCCTGCCTGAAGCTCTTGT
IL-18 (F)	ACTGGCTGTTCCCACAACGA
IL-18 (R)	CAGCACACCACAGGGGAGAA
NLRP3 (F)	GACACGAGTCCTGGTGACTTT
NLRP3 (R)	TCATCTTCAGCAGCAGCCCTT
TLR4 (F)	ATGCTACAGCTCACCTGGGG
TLR4 (R)	CTTCTGCCCGGTAAGGTCCA
TLR2 (F)	TGGTGCCCAGATGGCTAGTG
TLR2 (R)	AGGAAACAGTCCGCACCTCC
GAPDH (F)	GGAAAGCTGTGGCGTGATGG
GAPDH (R)	TACTTGGCAGGTTTCTCCAGG

Statistical analysis

The results of immunofluorescence (n=3), staining (n=3) and the PCR (n=4) experiments are expressed as mean ± SEM. For the staining experiments, the nuclei were counted using ImageJ software with ‘*Analyze particle*’ mode and the average MFI of 2-4 images randomly acquired from different fields of the experimental set were used to calculate the $\log_2$ FC [13]. The images that displayed background fluorescence were exempted from the analysis. Similarly, the PCR results were expresses as $\log_2$ FC with respect to the control. The statistical significance was assessed by one-way ANOVA following two-stage linear step-up procedure of Benjamini, Krieger and Yekutieli using GraphPad Prism software. The $p<0.05$ values were used to determine the significant difference between the experimental groups.

Results

Immunopositivity of protein mediators

The protein expression of proinflammatory receptor TLR2 was increased in the LDL (P=0.0478) and LPS treatment (P=0.1800) compared to the control; however, the increase was statistically not significant in

the LPS group. The level of TLR2 was significantly decreased in oxLDL group compared to LDL (P=0.0055) and LPS (P=0.0143) treatment groups; however, the decrease in oxLDL group was statistically not significant (P=0.1241) (**Figures 1A and 1H**). The protein expression of the proinflammatory TLR4 was decreased in LDL (P=0.4836), oxLDL (P=0.4986) and LPS (P=0.0868) groups compared to the control where the oxLDL group displayed decreased expression compared to LDL (P=0.2585) and LPS (P=0.2494) groups; however, the decrease was statistically not significant (**Figures 1A and 1I**). The protein expression of the DAMP HMGB1 was decreased in LDL (P=0.5391), oxLDL (P=0.2313) and LPS (P=0.5844) groups compared to the control and oxLDL group displayed decreased expression compared to LDL (P=0.4873) and LPS (P=0.4513) groups; however, the decrease was statistically not significant (**Figures 1B and 1J**). The protein level of proinflammatory receptor RAGE was increased in LDL (P=0.4041), oxLDL (P=0.5651) and LPS (P=0.3200) groups compared to the control and oxLDL group displayed increased expression compared to LDL (P=0.8544) and LPS (P=0.7341) groups; however, the increase was statistically not significant (**Figures 1B and 1K**). The protein expression of sterile inflammatory mediator ASC was decreased in LDL (P=0.5345) and increased in oxLDL (P=0.2433) and LPS (P=0.8038) groups compared to the control where the oxLDL group displayed increased expression compared to LDL (P=0.0850) and LPS (P=0.1649) groups; however, the alterations in the expression were statistically not significant (**Figures 1C and 1L**). The protein expression of sterile inflammatory mediator NLRP3 was significantly decreased in LDL (P=0.0020) and oxLDL (P=0.0020); however, the decrease in LPS (P=0.0709) was statistically not significant. Also, similar level of expression was observed between oxLDL (P=0.9966) and LPS (P=0.0672) group compared to the LDL group (**Figures 1C and 1M**). The protein expression of sterile inflammatory protease caspase 1 was decreased in LDL (P=0.6606), oxLDL (P=0.2879) and increased in LPS (P=0.8855) groups compared to the control and oxLDL group displayed decreased expression compared to LDL (P=0.5141) and LPS (P=0.2340) groups; however, were not statistically significant (**Figures 1D and 1N**). The level of inflammatory cytokine IL-1β was significantly decreased in LDL (P=0.0252) and increased in oxLDL (P=0.1139) and LPS (P=0.1226) groups compared to the control; however, the increase was statistically not significant. Moreover, the oxLDL (P=0.0019) and LPS (P=0.0021) groups displayed significantly higher expression compared to LDL (P=0.0850) (**Figures 1D and 1O**). The protein level of inflammatory receptor TREM1 was significantly increased in LDL (P=0.0415), oxLDL (P=0.0198) and LPS (P=0.0063) groups compared to the control and oxLDL group displayed similar expression compared to LDL (P=0.6466) and LPS (P=0.4626) groups (**Figures 1E and 1P**). The level of NF-κB was decreased in LDL (P=0.0988) and increased in oxLDL (P=0.1465) and LPS (P=0.0631) groups compared to the control; however, the increase was statistically not significant. In addition, the oxLDL (P=0.0084) and LPS (P=0.0038) groups displayed significantly higher expression compared to LDL (**Figures 1F and 1Q**). The level of inflammatory cytokine IL-18 was decreased in LDL (P=0.6951), oxLDL (P=0.2699) and LPS (P=0.6263) groups compared to the control and oxLDL group displayed decreased expression compared to LDL (P=0.4325) and LPS (P=0.9226) groups; however, the decrease was statistically not significant (**Figures 1G and 1R**).

Lipid intake

The lipid uptake and intracellular lipid droplets were increased in LDL (P=0.0953) and oxLDL (P=0.0044) treatment groups; however, the increase in LDL was statistically not significant. OxLDL group displayed increase in lipid uptake compared to LDL (P=0.0765) and LPS (P=0.0024) groups; however, the increase was statistically not significant in LDL group (**Figures 2A and 2B**).

Lipid peroxidation

Lipid peroxidation was more in the normal groups compared to the CuP treated controls (**Figures 2C-2F**). Lipid peroxidation was significantly higher in LDL (P=0.0111) and LPS (P=0.0377) groups compared to the respective CuP treatment groups; however, the increased level of lipid peroxidation is statistically not significant in oxLDL group (P=0.4529) compared to the corresponding CuP group. Also, similar level of peroxidation was observed in the control cells (P=0.7728) compared to the CuP control. Moreover, the level of lipid peroxidation in LDL group was higher than the oxLDL (P=0.6442) and LPS group (P=0.0153), however, the increase was statistically not significant in the oxLDL group. Also, the CuP-treated LPS group displayed decreased peroxidation compared to oxLDL group (P=0.0496). Interestingly, increased lipid peroxidation was observed in the LDL (P=0.1190), oxLDL (P=0.2727) and LPS (P=0.2253) groups; however, the increase was statistically not significant. Increased level of lipid peroxidation was displayed by CuP treated oxLDL group compared to the control CuP group; however, was statistically not significant. Additionally, similar level of peroxidation was observed in CuP treated LDL (P=0.4884) and LPS (P=0.5637) groups compared to the control CuP group.

Mitochondrial content

The mitochondrial content was significantly increased in oxLDL (P=0.0055) and LPS (P=0.0259) groups and was decreased in LDL group compared to the control; however, the decrease in mitochondrial density was statistically not significant in LDL (P=0.0704). Also, the LDL group displayed significant decrease in mitochondrial content when compared to oxLDL (P=0.0004) and LPS (P=0.0013) groups (**Figures 3A and 3B**).

Mitochondrial superoxide

The mitochondrial superoxide content was significantly decreased in LDL (P<0.0001), oxLDL (P<0.0001) and LPS (P<0.0001) groups compared to the control. Also, the mitochondrial superoxide level was significantly increased in oxLDL (P=0.0123), and LDL (P<0.0001) groups compared to LPS group. Moreover, the LDL group displayed significant decrease in mitochondrial superoxide when compared to oxLDL (P=0.0005) group (**Figures 3C and 3D**).

Mitochondrial pore transition

The calcein signal was significantly increased in LDL (P<0.0001), oxLDL (P<0.0001) and LPS (P<0.0001) groups compared to the control where oxLDL group displayed significant increase in calcein level compared to LDL (P<0.0001 which in turn was significantly decreased compared to LPS (P=0.0172). Also, the mitotracker signal was significantly increased in LDL (P<0.0001), oxLDL (P<0.0001) and LPS (P<0.0001) groups compared to the control where oxLDL group displayed significant increase in mitotracker signal compared to LDL (P<0.0001) which in turn was significantly decreased compared to LPS (P=0.0494) (**Figures 4A and 4C**). The increased level of calcein and mitotracker in oxLDL suggest the compromised mitochondrial membrane integrity with a concomitant increase in mitochondrial density.

Microtubule staining and cell spreading

ViaFlour staining revealed significant increase in the level of microtubules in the oxLDL (P=0.0202) group and decreased levels in LDL (P=0.1539) and LPS (P=0.8209) groups compared to the control; however, the decreased levels were statistically not significant. The microtubules were significantly increased in the oxLDL group than LDL (P=0.0021) and LPS (P=0.0141) groups (**Figures 4B and 4D**). The cellular area was significantly decreased in LDL (P=0.0431) group and significantly increased in oxLDL (P<0.0001) and LPS (P<0.0001) groups. Also, the cellular area was significantly increased in the oxLDL group than LDL (P<0.0001) and LPS (P=0.0545) groups (**Figures 4B and 4E**). Similarly, the cellular perimeter was significantly decreased in LDL (P=0.0336) group and significantly increased in oxLDL (P<0.0001) and LPS (P<0.0001) groups. Moreover, the cellular perimeter was significantly increased in the oxLDL group than LDL (P<0.0001) and LPS (P=0.0218) groups (**Figures 4B and 4E**).

mRNA transcription

The level of TLR4 mRNA transcript was significantly decreased in LDL (P<0.0001) and oxLDL (P=0.0002) groups and significantly increased in the LPS (P<0.0001) group compared to the control. Also, the oxLDL group displayed significant increase in TLR4 transcripts than the LDL (P=0.0260) group and significantly decreased level compared to the LPS (P<0.0001) group (**Figure 5A**). TLR2 transcripts were decreased in LDL (P=0.9894), oxLDL (P=0.0017) and LPS (P<0.0001) groups; however, the decreased expression in LDL group was statistically not significant. Moreover, the oxLDL group displayed significant decrease in TLR2 transcripts than the LDL (P=0.0018) group and significantly increased level compared to the LPS (P<0.0001) group (**Figure 5B**). The level of ASC transcript was significantly decreased in LDL (P=0.0343) and oxLDL (P=0.0329) groups and significantly increased in LPS (P<0.0001) group compared to the control. Also, the oxLDL group displayed similar level of expression compared to the LDL (P=0.9842) group and significantly decreased level compared to the LPS (P<0.0001) group (**Figure 5C**). NLRP3 was decreased in LDL (P=0.9402), oxLDL (P<0.0001) and LPS (P=0.0239) groups; however, the decreased expression in the LDL group was statistically not significant. In addition, the oxLDL group displayed significant decrease in NLRP3 transcripts than the LDL (P<0.0001) and LPS groups (P=0.0003) (**Figure 5D**). The level of IL-1β transcript was decreased in LDL (P=0.3285) group compared to the control;

however, was statistically not significant. OxLDL (P<0.0001) and LPS (P<0.0001) groups displayed a significant increase in IL-1β compared to the control. Moreover, the oxLDL group showed increased expression compared to the LDL (P<0.0001) and LPS (P<0.0001) groups (**Figure 5E**). The level of IL-18 mRNA transcript was decreased in LDL (P=0.0081) and oxLDL (P=0.5144) groups and significantly increased in the LPS (P<0.0001) group compared to the control; however, the decrease in oxLDL group was statistically not significant. Also, the oxLDL group displayed significant increase in IL-18 transcripts than the LDL (P=0.0328) group and significantly decreased level compared to the LPS (P<0.0001) group (**Figure 5F**).

Discussion

Atherosclerosis is driven by chronic inflammation sustained by the increased pool of proinflammatory cytokines and chemokines secreted by the macrophages at the site of the lesion. Furthermore, the key pro-atherogenic cytokines IL-18 and IL-1β are regulated by NLRP3 inflammasome [14]. However, the inhibition of NLRP3 by LDL and oxLDL in human macrophages during the early atheroma has been reported suggesting a counter mechanism of cell survival [2]. In our study, the RAW 264.7 macrophage cells challenged with a sub-lethal concentration of oxLDL revealed the upregulation of RAGE, and TREM1 receptors and the pro-inflammatory cytokine IL-1β. Surprisingly, the levels of DAMP molecule HMGB1, sterile inflammatory receptors TLR2 and TLR4, NLRP3 inflammasome mediators including caspase 1, and NLRP3 and the end-product cytokine IL-18 were decreased compared to untreated controls. Interestingly, the level of expression of the mediators in LPS-challenged groups were superior to the oxLDL group. Moreover, a similar trend was observed for the mediators at the transcript levels confirming the hypothesis. Hence, these results findings revealed the information on the mediators involved and the possible underlying mechanisms for the prevention of inflammation elicited by macrophages upon naïve encounter with oxLDL.

Interestingly, the two pro-inflammatory cytokines, IL-18 and IL-1β, derived from the same pathway exhibited distinct expression pattern by the RAW 264.7 macrophages at the transcript and protein level on encountering the oxLDL. Importantly, IL-18 has been reported to possess superior effects in triggering and sustaining inflammatory diseases including atherosclerosis compared to IL-1β [15] [16]. On the other hand, IL-1β is a pleotropic cytokine that elicits acute inflammatory response, procoagulant effects via the induction of tissue factor, and endothelial permeability. These biological effects are prevalent in the early phase of atherosclerosis signifying the upregulation [17]. However, the ratio of IL-18 and IL-1β may vary depending on the cell types. For example, our previous investigations revealed the increased level of IL-18 than IL-1β in cultured arterial smooth muscle cells upon treatment with oxLDL (data not shown in this article). Overall, the macrophages upregulate IL-1β with a concomitant down regulation of IL-18, NLRP3 mediators and TLRs suggesting the possible alternative mechanism IL-1β activation which warrants further detailed investigation.

The foam cell formation by macrophages is a major hallmark of atherosclerotic lesions resulting from the increased uptake of oxLDL and subsequent deposition in the cytoplasm coupled with the decreased

efflux of cholesterol [18]. Moreover, the increased expression of scavenging receptors (SR) including CD36 (also called fatty acid translocase), SR-A1 and lectin-like oxLDL receptor-1 (LOX-1) by the macrophages has been intimately associated with foam cell formation in atherosclerosis [18] [19]. Substantially, the macrophages treated with oxLDL displayed increased intracellular lipids suggesting the active operation of SR signaling which is beyond the focus of this study; however, warranting further investigations. Additionally, the intracellular functions of oxLDL in triggering atheromatous lesions are currently unknown requiring detailed future studies.

OxLDL is likely to alter the cellular biochemistry facilitating the increased peroxidation of free and membrane bound lipids compromising the membrane integrity resulting in the lysis of cells/organelles [20]. Apart from lipid peroxidation, oxLDL promotes cytotoxicity by iron-mediated free radical formation further contributing to macrophage cytotoxicity [21]. Interestingly, several oxysterols including 7β-hydroxyperoxycholesterol have been identified as the cytotoxic components contained in oxLDL; however, the implications of oxysterols in foam cell formation by macrophages in atherosclerosis are largely unknown [22] [23]. As expected, the lipid peroxidation level was increased in the oxLDL treatment in RAW 264.7 macrophages suggesting the pro-atheromatous milieu. Importantly, a seminal report demonstrated that the oxLDL promotes the formation of peroxides compromising the mitochondrial integrity; however, suppresses the formation of superoxide [24]. Additionally, our data revealed that the decreased mitochondrial membrane potential as evidenced by the increased calcein fluorescence suggesting that the compromised mitochondrial membrane drives impaired calcium transit [25]. Surprisingly, the mitochondrial density was increased upon the treatment with oxLDL suggesting the adaptive mechanisms to nullify the pathological effects by substantially increasing the number of mitochondria [26]. Interestingly, our findings revealed decreased level of reactive superoxide upon oxLDL treatment in macrophages suggesting that the pathological effects of oxLDL in macrophages are mediated by lipid peroxidation and mitochondrial dysfunction but not through reactive superoxide radicals.

The increased lipoprotein burden imparts the alterations in cellular morphology resulting in hypertrophy [27] [28]. In macrophages, the cellular hypertrophy has been implicated to the lysosomal load of oxLDL [29] and has been intimately associated with atherosclerosis [30] [31]. In addition, oxLDL has been reported to induce uncontrolled and robust actin polymerization via 12/15-Lipoxygenase activity leading to dramatic changes in the cytoskeletal organization in macrophages [32]. Interestingly, our study revealed increased microtubules with a concomitant increase in the cellular area and perimeter of macrophages on encountering oxLDL correlating the pathological drive for atherosclerosis; however, the information regarding the underlying molecular implications is unavailable which warrants further investigations.

The five major genes that were downregulated in RAW 264.7 macrophages on encountering oxLDL (TLR4, TLR2, ASC, NLRP3 and IL18) are the central players of inflammasome signaling and are involved in the initiation and progression of atherosclerosis. These downregulated genes are associated with 120 pathways as correlated by ORA (Over Representation Analysis) based on human Gene Ontology: Biological Processes (GO:BP) (Fig. 6A) (**Supplementary Table 1**). Volcano and funnel plots revealed that

the predominant biological events associated with the downregulated genes are primarily involved in immune and stress responses (Figs. 6B and 6D) (**Supplementary Table 1**). The artery-specific interactions revealed the network associated with 120 pathways and 96 genes (Figs. 6C) (**Supplementary Table 1**). The pathways and interconnected genes associated with TLR4, TLR2, ASC, NLRP3 and IL18 are mostly involved in immune responses and stress homeostasis signifying the downregulation of these processes suggesting the suppression of inflammatory responses upon encountering oxLDL by macrophages. Hence, the initial phase of oxLDL action is possibly driven through the suppression of sterile inflammatory responses in the macrophages warranting further detailed investigations.

The involvement of oxLDL in triggering sterile inflammatory responses in the macrophages during the progression of atherosclerosis has been established; however, our findings revealed that the expression status of key sterile mediators and the macrophage response during the initial phase of oxLDL exposure tend toward the prevention of inflammation. Moreover, the literature regarding the anti-inflammatory responses elicited by oxLDL treatment is rare in the literature suggesting the possible survival response in the macrophages. Even though the findings are novel, the study was not exempted from limitations warranting further investigations. The potential pitfalls include (1) the study focused on the acute responses of oxLDL whereas atherosclerosis pathology is driven by the chronic exposure of oxLDL with vascular and immune cells, (2) the phenotype of macrophages used in this study was not defined, and (3) the expression status of SRs was not established. Nonetheless, the present study unveils novel insights into the survival responses of macrophages on encountering oxLDL and the further understanding of which would open novel translational opportunities in the management of atherosclerosis.

Conclusion

The RAW 264.7 macrophage cells displayed a decreased expression of the key mediators (TLR4, TLR2, ASC, NLRP3 and IL18) associated with NLRP3 inflammasome at protein and transcript level upon encountering oxLDL. The biological responses including lipid uptake, lipid peroxidation, superoxide production and mitochondrial membrane potential were decreased whereas cellular hypertrophy, and mitochondrial density were decreased in the oxLDL-treated macrophages compared to the control. Overall, the findings revealed that the expression status of key sterile mediators and the macrophage response during the initial phase of oxLDL exposure tend toward the prevention of inflammation and the further understanding of which would open novel translational opportunities in the management of atherosclerosis.

Declarations

Ethics approval and consent to participate:

Not applicable.

Consent for publication:

All the authors have read the manuscript and consented for publication.

Availability of data and materials:

Data with the raw counts matrices and annotation are available upon request from the authors through proper channels.

Competing Interest:

All the authors have read the manuscript and declare no conflict of interest. No writing assistance was utilized in the production of this manuscript.

Funding:

The research work of FT is supported by the startup funds from WU and DK Agrawal is supported by research grants R01 HL144125 and R01HL147662 from the National Institutes of Health, USA.

Authors' contributions:

FT – conceptualization, design, methodology, data generation, analysis, supervision, funding and manuscript preparation and editing; BK – data generation, analysis, supervision, and manuscript preparation and editing; MG – data generation, analysis, supervision, and manuscript preparation and editing; OA – data generation, analysis, supervision, and manuscript preparation and editing; DA – conceptualization, design, analysis, supervision, funding and manuscript preparation and editing.

Acknowledgements:

FT is thankful to WU for the startup funds and DA is grateful to National Institutes of Health, USA for funding.

References

1. Jin, Ying, and Jian Fu. 2019. Novel Insights Into the NLRP3 Inflammasome in Atherosclerosis. *Journal of the American Heart Association* 8. American Heart Association: e012219. https://doi.org/10.1161/JAHA.119.012219.
2. Nurmi, Katariina, Katri Niemi, Ilona Kareinen, Kristiina Silventoinen, Martina B Lorey, Yan Chen, Vesa-Petteri Kouri, et al. 2021. Native and oxidised lipoproteins negatively regulate the serum amyloid A-

induced NLRP3 inflammasome activation in human macrophages. *Clinical & Translational Immunology* 10: e1323. https://doi.org/10.1002/cti2.1323.

3. Moore, Kathryn J., and Ira Tabas. 2011. Macrophages in the pathogenesis of atherosclerosis. *Cell* 145: 341–355. https://doi.org/10.1016/j.cell.2011.04.005.
4. Thankam, Finosh G., Zachary K. Roesch, Matthew F. Dilisio, Mohamed M. Radwan, Anuradha Kovilam, R. Michael Gross, and Devendra K. Agrawal. 2018. Association of Inflammatory Responses and ECM Disorganization with HMGB1 Upregulation and NLRP3 Inflammasome Activation in the Injured Rotator Cuff Tendon. *Scientific Reports* 8: 1–14. https://doi.org/10.1038/s41598-018-27250-2.
5. Thankam, Finosh G., Matthew F. Dilisio, Kaitlin A. Dougherty, Nicholas E. Dietz, and Devendra K. Agrawal. 2016. Triggering receptor expressed on myeloid cells and 5'adenosine monophosphate-activated protein kinase in the inflammatory response: a potential therapeutic target. *Expert Review of Clinical Immunology* 12. Taylor & Francis: 1239–1249. https://doi.org/10.1080/1744666X.2016.1196138.
6. Thankam, Finosh G., Matthew F. Dilisio, Nicholas E. Dietz, and Devendra K. Agrawal. 2016. TREM-1, HMGB1 and RAGE in the Shoulder Tendon: Dual Mechanisms for Inflammation Based on the Coincidence of Glenohumeral Arthritis. *PLoS ONE* 11. https://doi.org/10.1371/journal.pone.0165492.
7. Li, Kang, David K. Wong, Fu Sang Luk, Roy Y. Kim, and Robert L. Raffai. 2018. Isolation of Plasma Lipoproteins as a Source of Extracellular RNA. In *Extracellular RNA*, ed. Tushar Patel, 1740:139–153. Methods in Molecular Biology. New York, NY: Springer New York. https://doi.org/10.1007/978-1-4939-7652-2_11.
8. Viola, Manuela, Barbara Bartolini, Davide Vigetti, Evgenia Karousou, Paola Moretto, Sara Deleonibus, Tatsuya Sawamura, et al. 2013. Oxidized Low Density Lipoprotein (LDL) Affects Hyaluronan Synthesis in Human Aortic Smooth Muscle Cells. *Journal of Biological Chemistry* 288: 29595–29603. https://doi.org/10.1074/jbc.M113.508341.
9. Thankam, Finosh G., Chandra S. Boosani, Matthew F. Dilisio, and Devendra K. Agrawal. 2017. MicroRNAs associated with inflammation in shoulder tendinopathy and glenohumeral arthritis. *Molecular and Cellular Biochemistry*. https://doi.org/10.1007/s11010-017-3097-7.
10. Thankam, Finosh G., Nicholas K. Larsen, Ann Varghese, Thao-Nguyen Bui, Matthew Reilly, Robert J. Fitzgibbons, and Devendra K. Agrawal. 2021. Biomarkers and heterogeneous fibroblast phenotype associated with incisional hernia. *Molecular and Cellular Biochemistry* 476: 3353–3363. https://doi.org/10.1007/s11010-021-04166-6.
11. Thankam, Finosh G., Isaiah S. Chandra, Anuradha N. Kovilam, Connor G. Diaz, Benjamin T. Volberding, Matthew F. Dilisio, Mohamed M. Radwan, R. Michael Gross, and Devendra K. Agrawal. 2018. Amplification of Mitochondrial Activity in the Healing Response Following Rotator Cuff Tendon Injury. *Scientific Reports* 8: 1–14. https://doi.org/10.1038/s41598-018-35391-7.
12. Thankam, Finosh G., Isaiah S. Chandra, Anuradha N. Kovilam, Connor G. Diaz, Benjamin T. Volberding, Matthew F. Dilisio, Mohamed M. Radwan, R. Michael Gross, and Devendra K. Agrawal.

2018. Amplification of Mitochondrial Activity in the Healing Response Following Rotator Cuff Tendon Injury. *Scientific Reports* 8. https://doi.org/10.1038/s41598-018-35391-7.

13. Thankam, Finosh G., Victoria E. D. Wilson, Mohamed M. Radwan, Aleem Siddique, and Devendra K. Agrawal. 2022. Involvement of ischemia-driven 5-lipoxygenase-resolvin-E1-chemokine like receptor-1 axis in the resolution of post-coronary artery bypass graft inflammation in coronary arteries. *Molecular Biology Reports*. https://doi.org/10.1007/s11033-022-07143-4.
14. Ding, Wenyuan, Jiamin Li, Lili Wang, Mingming Zhang, and Fei Zheng. 2020. ClC-2 inhibition prevents macrophage foam cell formation by suppressing Nlrp3 inflammasome activation. *Bioscience, Biotechnology, and Biochemistry* 84: 2096–2103. https://doi.org/10.1080/09168451.2020.1793294.
15. Dinarello, Charles, Daniela Novick, SooHun Kim, and Gilles Kaplanski. 2013. Interleukin-18 and IL-18 Binding Protein. *Frontiers in Immunology* 4: 289. https://doi.org/10.3389/fimmu.2013.00289.
16. Blankenberg, Stefan, Laurence Tiret, Christoph Bickel, Dirk Peetz, François Cambien, Jürgen Meyer, and Hans J. Rupprecht. 2002. Interleukin-18 Is a Strong Predictor of Cardiovascular Death in Stable and Unstable Angina. *Circulation* 106. American Heart Association: 24–30. https://doi.org/10.1161/01.CIR.0000020546.30940.92.
17. Puhlmann, Markus, David M Weinreich, Jeffrey M Farma, Nancy M Carroll, Ewa M Turner, and H Richard Alexander. 2005. Interleukin-1β induced vascular permeability is dependent on induction of endothelial Tissue Factor (TF) activity. *Journal of Translational Medicine* 3: 37. https://doi.org/10.1186/1479-5876-3-37.
18. Chistiakov, Dimitry A., Yuri V. Bobryshev, and Alexander N. Orekhov. 2016. Macrophage-mediated cholesterol handling in atherosclerosis. *Journal of Cellular and Molecular Medicine* 20: 17–28. https://doi.org/10.1111/jcmm.12689.
19. Ding, Zufeng, Shijie Liu, Xianwei Wang, Sue Theus, Xiaoyan Deng, Yubo Fan, Sichang Zhou, and Jawahar L Mehta. 2018. PCSK9 regulates expression of scavenger receptors and ox-LDL uptake in macrophages. *Cardiovascular Research* 114: 1145–1153. https://doi.org/10.1093/cvr/cvy079.
20. Reid, V. C., and M. J. Mitchinson. 1993. Toxicity of oxidised low density lipoprotein towards mouse peritoneal macrophages in vitro. *Atherosclerosis* 98: 17–24. https://doi.org/10.1016/0021-9150(93)90219-k.
21. Coffey, M. D., R. A. Cole, S. M. Colles, and G. M. Chisolm. 1995. In vitro cell injury by oxidized low density lipoprotein involves lipid hydroperoxide-induced formation of alkoxyl, lipid, and peroxyl radicals. *The Journal of Clinical Investigation* 96: 1866–1873. https://doi.org/10.1172/JCI118232.
22. Yuan, X. M., W. Li, U. T. Brunk, H. Dalen, Y. H. Chang, and A. Sevanian. 2000. Lysosomal destabilization during macrophage damage induced by cholesterol oxidation products. *Free Radical Biology & Medicine* 28: 208–218. https://doi.org/10.1016/s0891-5849(99)00220-8.
23. Chisolm, G. M., G. Ma, K. C. Irwin, L. L. Martin, K. G. Gunderson, L. F. Linberg, D. W. Morel, and P. E. DiCorleto. 1994. 7 beta-hydroperoxycholest-5-en-3 beta-ol, a component of human atherosclerotic lesions, is the primary cytotoxin of oxidized human low density lipoprotein. *Proceedings of the*

National Academy of Sciences of the United States of America 91: 11452–11456. https://doi.org/10.1073/pnas.91.24.11452.

24. Asmis, Reto, and Jim G. Begley. 2003. Oxidized LDL Promotes Peroxide-Mediated Mitochondrial Dysfunction and Cell Death in Human Macrophages. *Circulation Research* 92. American Heart Association: e20–e29. https://doi.org/10.1161/01.RES.0000051886.43510.90.
25. Mazière, Cécile, Patrice Morlière, Ziad Massy, Said Kamel, Christophe Louandre, Marie-Alix Conte, and Jean-Claude Mazière. 2005. Oxidized low-density lipoprotein elicits an intracellular calcium rise and increases the binding activity of the transcription factor NFAT. *Free Radical Biology & Medicine* 38: 472–480. https://doi.org/10.1016/j.freeradbiomed.2004.10.028.
26. Thankam, Finosh G., Isaiah S. Chandra, Anuradha N. Kovilam, Connor G. Diaz, Benjamin T. Volberding, Matthew F. Dilisio, Mohamed M. Radwan, R. Michael Gross, and Devendra K. Agrawal. 2018. Amplification of Mitochondrial Activity in the Healing Response Following Rotator Cuff Tendon Injury. *Scientific Reports* 8: 17027. https://doi.org/10.1038/s41598-018-35391-7.
27. Wattis, J. A. D., B. O'Malley, H. Blackburn, L. Pickersgill, J. Panovska, H. M. Byrne, and K. G. Jackson. 2008. Mathematical Model for Low Density Lipoprotein (LDL) Endocytosis by Hepatocytes. *Bulletin of Mathematical Biology* 70: 2303–2333. https://doi.org/10.1007/s11538-008-9347-9.
28. Božič, Bojan, Špela Zemljič Jokhadar, Luka Kristanc, and Gregor Gomišček. 2020. Cell Volume Changes and Membrane Ruptures Induced by Hypotonic Electrolyte and Sugar Solutions. *Frontiers in Physiology* 11: 1555. https://doi.org/10.3389/fphys.2020.582781.
29. Dawodu, Damilola, Margret Patecki, Jan Hegermann, Inna Dumler, Hermann Haller, and Yulia Kiyan. 2018. oxLDL inhibits differentiation and functional activity of osteoclasts via scavenger receptor-A mediated autophagy and cathepsin K secretion. *Scientific Reports* 8. Nature Publishing Group: 11604. https://doi.org/10.1038/s41598-018-29963-w.
30. Alexander, Matthew R., Joshua W. Knowles, Toshio Nishikimi, and Nobuyo Maeda. 2003. Increased Atherosclerosis and Smooth Muscle Cell Hypertrophy in Natriuretic Peptide Receptor A−/− Apolipoprotein E−/− Mice. *Arteriosclerosis, thrombosis, and vascular biology* 23: 1077–1082. https://doi.org/10.1161/01.ATV.0000071702.45741.2E.
31. Grootaert, Mandy O J, and Martin R Bennett. 2021. Vascular smooth muscle cells in atherosclerosis: time for a re-assessment. *Cardiovascular Research* 117: 2326–2339. https://doi.org/10.1093/cvr/cvab046.
32. Miller, Yury I., Dorothy S. Worrall, Colin D. Funk, James R. Feramisco, and Joseph L. Witztum. 2003. Actin Polymerization in Macrophages in Response to Oxidized LDL and Apoptotic Cells: Role of 12/15-Lipoxygenase and Phosphoinositide 3-Kinase. *Molecular Biology of the Cell* 14. American Society for Cell Biology (mboc): 4196–4206. https://doi.org/10.1091/mbc.e03-02-0063.

Figures

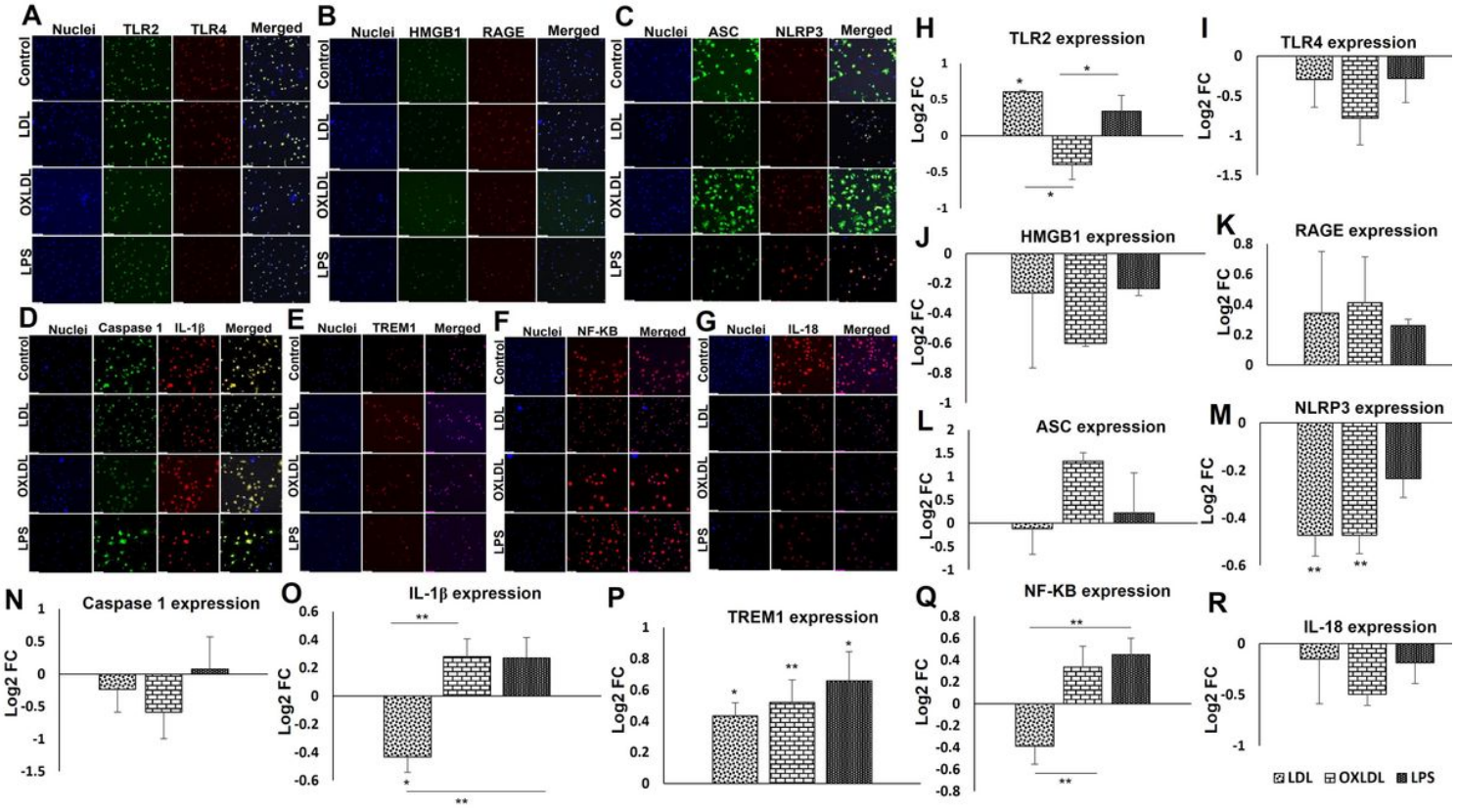

Figure 1

Representative images for the (A-D) immuno-double staining on the RAW264.7 macrophages for the expression of TLR2 and TLR4, HMGB1 and RAGE, ASC and NLRP3, Caspase 1 and IL1β showing the altered expression in the LDL, oxLDL and LPS treatment groups, (E-G) immunostaining on RAW264.7 macrophages for the expression of and TREM1, NF-κB, and IL-18 showing the altered expression in the LDL and oxLDL treatment group vessels. Images in the left column of each panel show nuclear staining with DAPI; the images in the middle column/s show expression of proteins while the images in the right column show overlay staining with DAPI. Images were acquired at 20x magnification. (H-R) The quantification of gene expression expressed as Log2 FC where the graph represents mean values with standard error. The statistical significance based on one-way ANOVA test is represented in the figure (** P<0.05, ** P<0.01, and unlabeled are non-significant*).

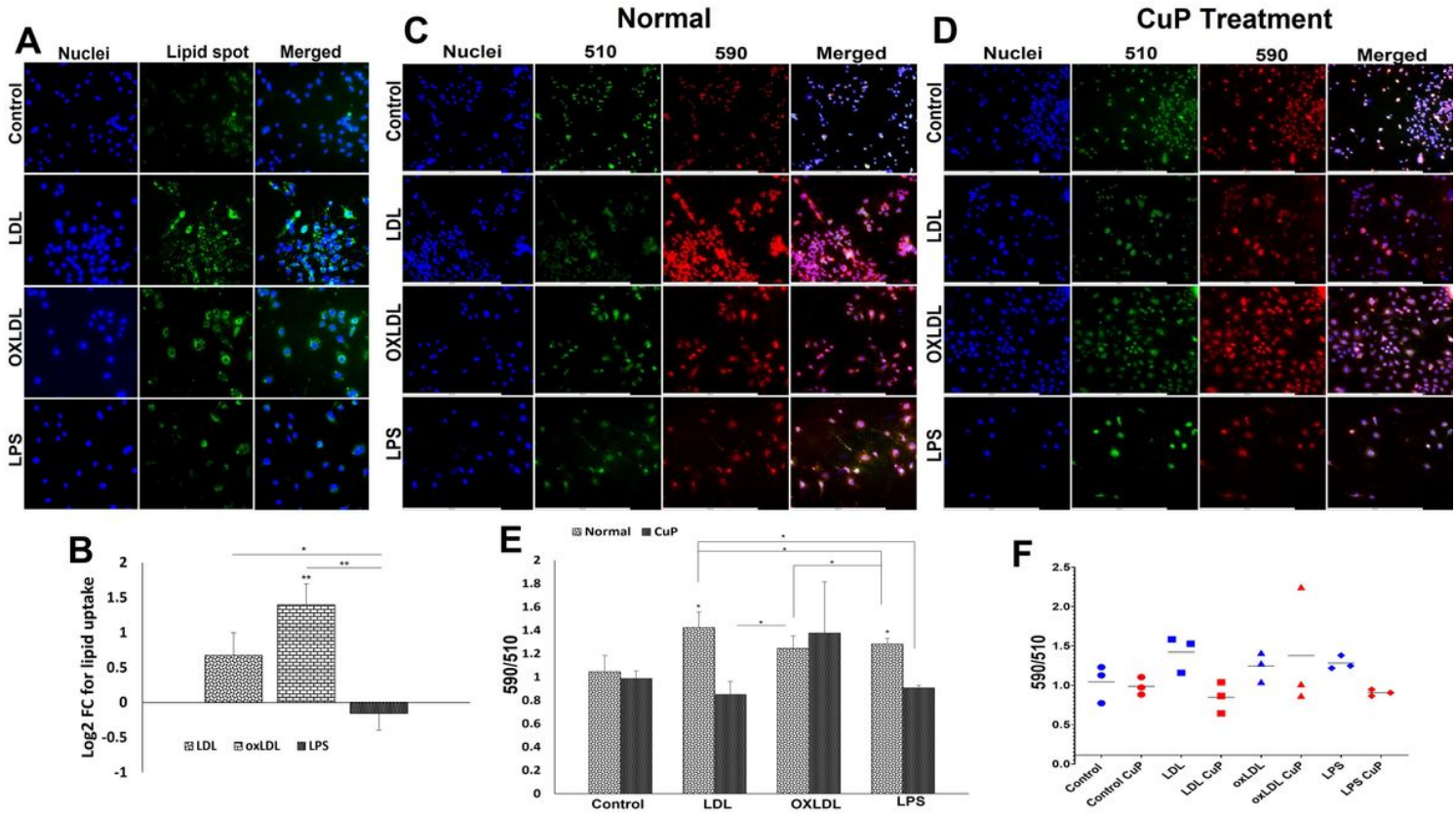

Figure 2

Representative images for the lipid droplet staining: (A) RAW 264.7 cells treated with LPS, LDL and oxLDL control. Images in the first row represent the control group, second row represents LDL group, third row represent the oxLDL treatment group and at the bottom row represent LDL treatment group. Images in the first panel show nuclear staining with DAPI; the images in the middle panel lipid droplet staining and the right panel shows overlay staining with DAPI. (B) The quantification of lipid droplets where the graph represents mean values with standard error. (C) and (D) Representative images for the lipid peroxidation staining: (C) RAW 264.7 cells treated with LPS, LDL and oxLDL control and (D) RAW 264.7 cells treated with LPS, LDL and oxLDL along with CuP. Images in the first row represent the control group, second row represents LDL group, third row represent the oxLDL treatment group and at the bottom row represent LDL treatment group. Images in the first panel show nuclear staining with DAPI; the images in the middle panels show intensities at 590 and 510 and the right panel shows overlay staining with DAPI. Images were acquired at 20x magnification. (E) The quantification of lipid peroxidation based on 590/510 ratio where the graph represents mean values with standard error. (F) Scatter plot showing the trend of lipid peroxidation in normal and CuP treatment group. The statistical significance based on one-way ANOVA test is represented in the figure (** P<0.05,* and *unlabeled are non-significant*).

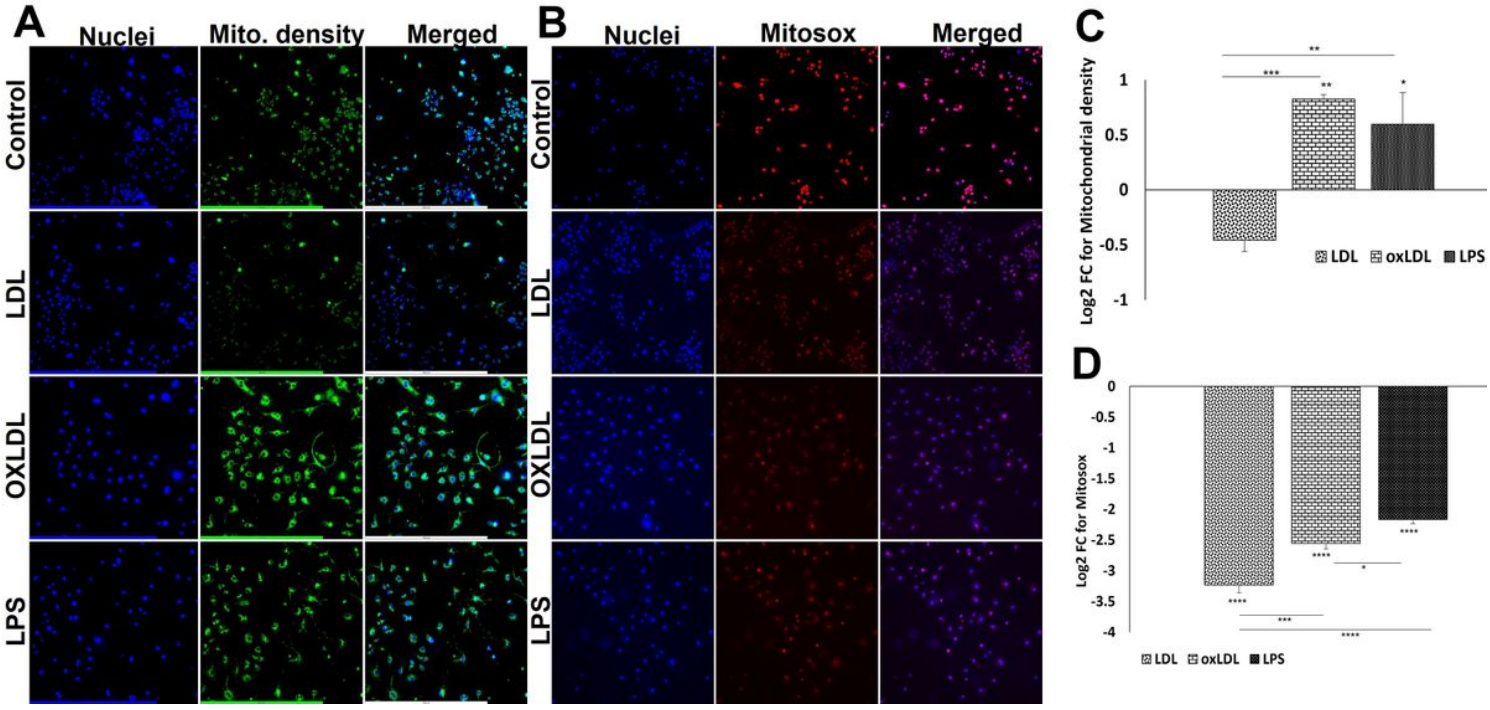

Figure 3

(A) Representative images for the MitoView™ Green staining in RAW 264.7 cells treated with LPS, LDL and oxLDL control. Images in the first row represent the control group, second row represents LDL group, third row represent the oxLDL treatment group and at the bottom row represent LDL treatment group. Images in the first panel show nuclear staining with DAPI; the images in the middle panel mitochondrial staining and the right panel shows overlay staining with DAPI. Images were acquired at 20x magnification. (B) The quantification of mitochondrial contents where the graph represents mean values with standard error. (C) Representative images for the Mitosox red staining in RAW 264.7 cells treated with LPS, LDL and oxLDL control. Images in the first row represent the control group, second row represents LDL group, third row represent the oxLDL treatment group and at the bottom row represent LDL treatment group. Images in the first panel show nuclear staining with DAPI; the images in the middle panel mitosox staining and the right panel shows overlay staining with DAPI. Images were acquired at 10x magnification. (D) The quantification of mitochondrial superoxide where the graph represents mean values with standard error. The statistical significance based on one-way ANOVA test is represented in the figure (** P<0.05, *** P<0.001, **** P<0.0001 and unlabeled are non-significant*).

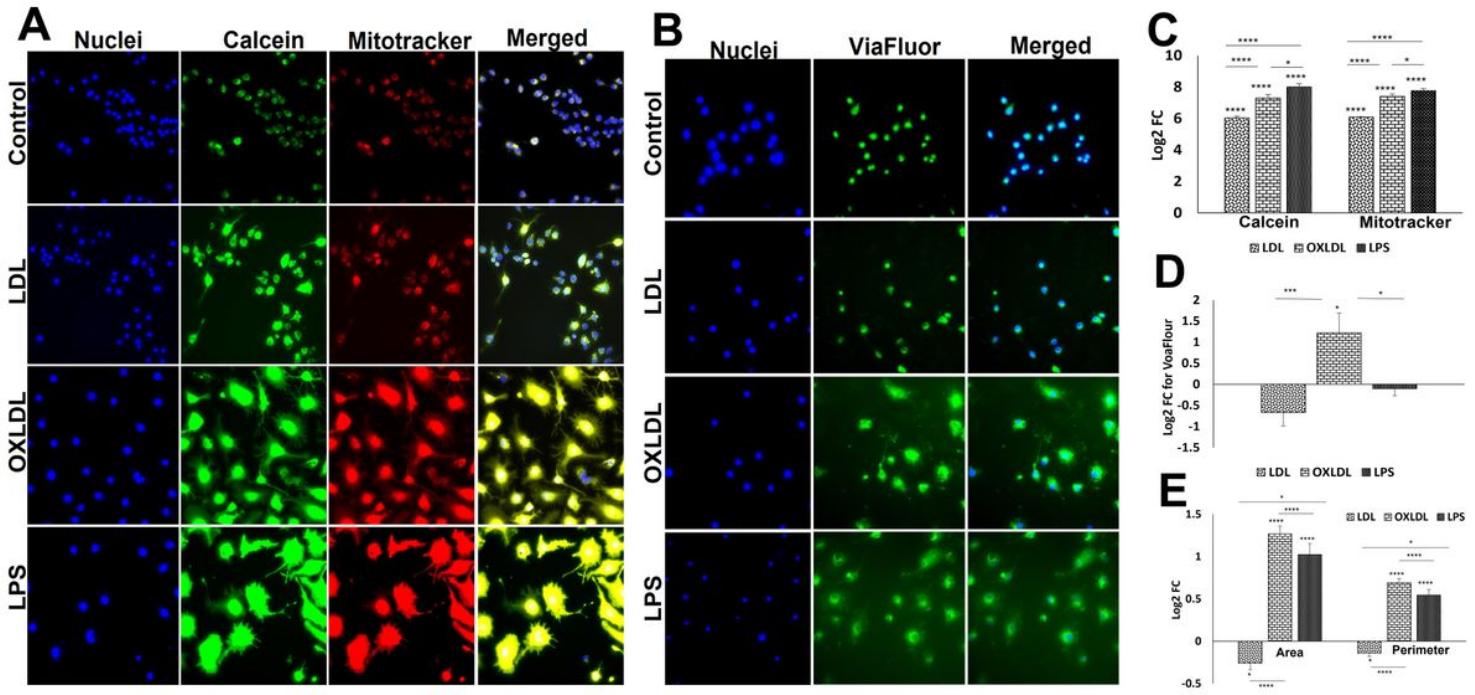

Figure 4

(A) Representative images for the mitochondrial pore transition staining in RAW 264.7 cells treated with LPS, LDL and oxLDL control. Images in the first row represent the control group, second row represents LDL group, third row represent the oxLDL treatment group and at the bottom row represent LDL treatment group. Images in the first panel show nuclear staining with DAPI; the images in the middle panels represent calcein and MitoTracker staining, and the right panel shows overlay staining with DAPI. Images were acquired at 20x magnification. (B) Representative images for the ViaFluor staining in RAW 264.7 cells treated with LPS, LDL and oxLDL control. Images in the first row represent the control group, second row represents LDL group, third row represent the oxLDL treatment group and at the bottom row represent LDL treatment group. Images in the first panel show nuclear staining with DAPI; the images in the middle panel represents ViaFlour staining, and the right panel shows overlay staining with DAPI. Images were acquired at 20x magnification. (C) and (D) The quantification of mitochondrial pore transition and microtubules respectively where the graph represents mean values with standard error. (E) The quantification of cellular area and perimeter where the graph represents mean values with standard error. The statistical significance based on one-way ANOVA test is represented in the figure (** P<0.05, *** P<0.001, **** P<0.0001 and unlabeled are non-significant*).

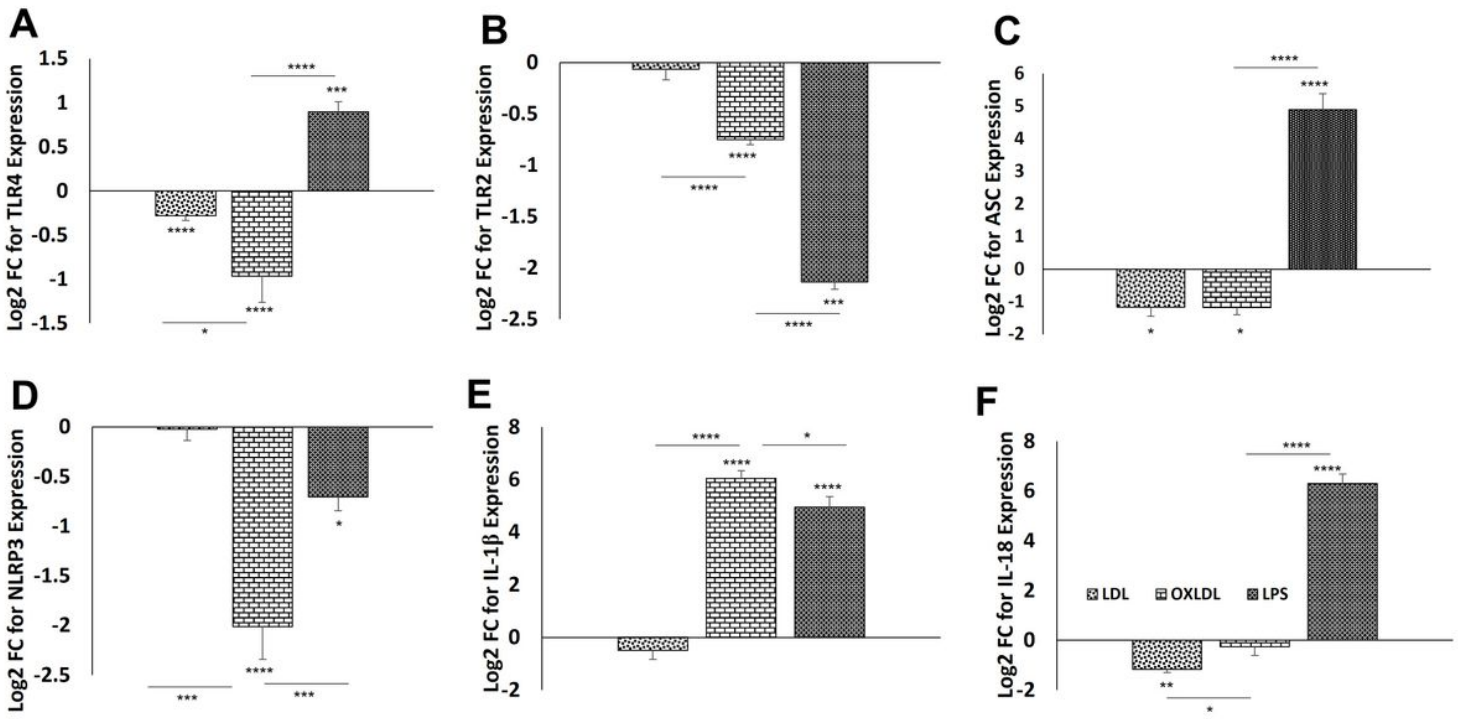

Figure 5

(A-F) qRT-PCR analysis for the mRNA expression of TLR4, TLR2, ASC, NLRP3, IL1β and IL18 cultured under ISC and ISC/R with respect to control. The results were expressed as log2 FC of expression relative to control. The statistical significance based on one-way ANOVA test is represented in the figure (** P<0.05, *** P<0.001, **** P<0.0001 and unlabeled are non-significant*).

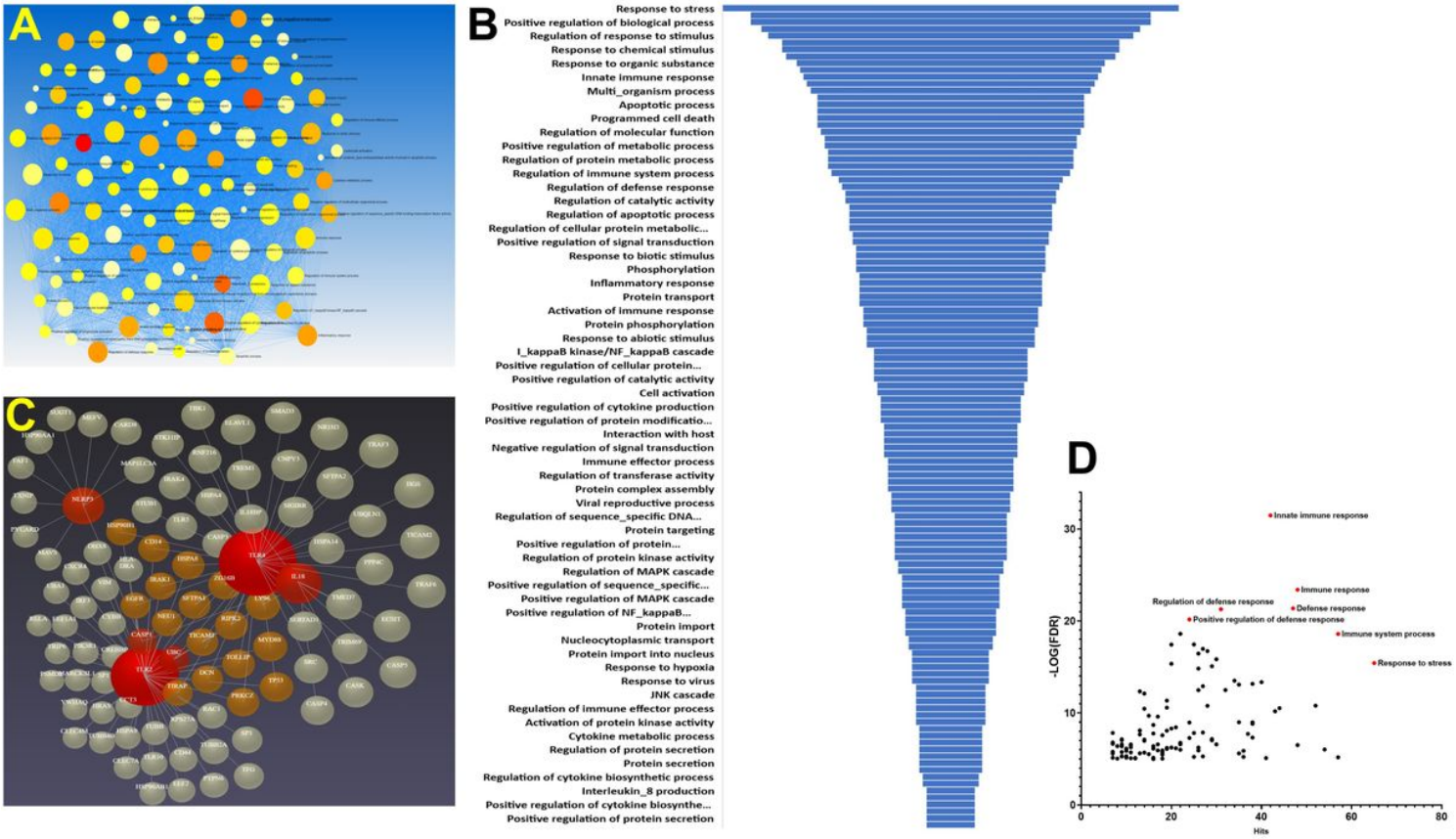

Figure 6

(**A**) ORA network visualization showing the interconnectivity of biological processes (GO: BP) based on the 5 input genes. (**B**) Funnel diagram displaying the total interactions for each biological process connected to the 5 input genes (*P<0.05 for all hits*). (**C**) 3D visualization based on the Force-directed map showing the crosstalk between 96 genes associated with the 5 regenerative input genes. (**D**) Volcano plot showing the key biological processes based on the -Log (FDR).

Supplementary Files

This is a list of supplementary files associated with this preprint. Click to download.

- Supplementarytable1.docx